ARTECH CORP.
14554 Lee Road • Chantilly, Virginia 22021-1632
(703) 378-7263 • Washington, D.C. Metro (703) 968-TEST • Fax (703) 378-7274

CHEMICAL AND METALLURGICAL ANALYSIS OF A RUPTURED DOT-3AL SPECIFICATION COMPRESSED GAS CYLINDER

BY

Vishwanath Sahay
Paul J. Lare

December 15, 1994

Prepared for:

U.S. DOT/RSPA
400 7th Street, S.W.,
Washington, D.C. 20590-0001

Order No. DTRS56-94-P-70365

ARTECH File No. 9509.002

INTRODUCTION

Three pieces of a ruptured DOT-3AL specification compressed gas cylinder, made from 6351-T6 aluminum alloy, were submitted to ARTECH for examination. See the Appendix I for chain of custody. Reportedly, about 7 million of such cylinders are currently in service. Sudden rupture of these cylinders, without any sign of warning, poses potential risk of personal injuries and/or property damage. This report summarizes findings of chemical and metallurgical examinations of the ruptured cylinder, performed by ARTECH.

EXAMINATION OF THE CYLINDER IN AS-RECEIVED CONDITION

General conditions and markings on the fractured pieces of the cylinder are presented in figures 1-13. Almost one half of the dome part of the cylinder had fractured off during the failure process.

The subject cylinder had been manufactured by LUXFER USA. It bore markings such as CTC/DOT-3AL 3000 and P20860 LUXFER 11A82 on its dome part. The last internal inspection of the cylinder had been performed in May 1994 by Scuba Sports of Sunrise, Florida; this inspection "expires 1 year from date indicated." No indications of any mechanical damage and/or corrosion activities were observed which might have aided the failure process.

Two smaller pieces were returned intact to Mr. Vinjamuri on October 27, 1994, for fracture toughness testing.

DIMENSIONAL MEASUREMENT:

A grid, 30° (circumferential) x 2" (axial), was laid on the outer surface of the cylinders in order to locate measurements and specimen layout. Circumferential divisions were marked 0-11, 0 being coincident to ⏃ mark near the cylinder bottom (see figure 6); axial divisions were marked A-M, A being at the top lip of the cylinder. A typical view of the grid structure is shown in figure 14. Axial divisions between A-B and B-C were further divided in four equal parts (i.e. A1-A4 and B1-B4). A micrometer with rounded contact heads was used for thickness measurements. Diameter and length measurements were performed using a measuring tape (see Table I for details).

TABLE I
DIMENSIONAL MEASUREMENTS, INCH

Location	Outside Diameter	Thickness	Length
At Grid Point			
0A1		0.3479	
1A1		0.3510	
2A1		0.3540	
3A1		0.3514	
4A1		0.3487	
5A1		0.3449	
0A2		1.3170	
0A3		1.1700	
0A4		0.8090	
9D		0.5250	
At Line			
D	7.304		
F	7.285		
H	7.285		
J	7.285		
L	7.285		
0			26
1			26
2			26
3			26
4			26
5			26
6			23 7/8

7			22 1/4
8			20 3/4
9			20 1/2
10			21 5/8
11			23 1/8

NOTE: Outside surface bend at the fracture face end of lines 7, 8, 9 and 10 was observed.

Straightness of the cylinder was documented by abutting a 90° metallic ruler against its outer surface and photographing the gap along its length (see figures 14-17).

CHEMICAL ANALYSIS

Two samples for chemical analysis were drilled (through thickness) from locations shown in figure 18A after removing coating/paint layer: one from near OC grid point (in straight part of the cylinder) and another from near OA2 grid point (in thick section near the neck of the cylinder). Analysis was performed per ASTM E34 Standard Method. Description of the test method is presented in the Appendix II. The test result is presented in Table II.

Table II
Chemical Composition, Wt %

Sample ID	Si	Fe	Cu	Mn	Mg	Zn	Ti	Bi	Pb	Sn	Cd
At OA2 Grid Point (Neck Region)	.76	.21	.02	.52	.63	.03	.09	.03	.06	.09	.001
At OC Grid Point (Barrel Region)	.77	.19	.02	.51	.63	.03	.09	.03	.05	.09	.001
Al 6351	$^{.70}/_{1.30}$	≤.50	≤.10	$^{.40}/_{.80}$	$^{.40}/_{.80}$	≤.20	≤.20	*	*	*	*

*Each element not to exceed 0.05%, total not to exceed 0.15%.

Chemical composition of the subject cylinder meets the standard requirements of an Al 6351 alloy except being rich in Lead (Pb), Bismuth (Bi), and Tin (Sn).

A repeat analysis, using the same technique as above, of a sample drilled from the core of the barrel part of the cylinder was performed to recheck Pb, Bi and Sn contents. The result is as follows: Pb-0.05%, Bi-0.05% and Sn-0.17%. Under a different task, Pb, Bi and Sn contents are being determined using a referee technique.

FRACTURE SURFACE EXAMINATION

The fractured part of the cylinder was removed from the main barrel for examination; a through cut was made between the circumferential lines D and E for the purpose. Figure 18B shows the location of the cut. A macro view of the main crack front is presented in figure 19. Optical microscopic examination revealed fracture features being identical on either side of the threaded hole. Upon approval of the COTR, side A of the fracture front was used for detailed fractography; side B was used for metallographic examination (figure 19). Side A of the fracture front was removed and cut in three 3-inch segments for analysis. Referring to figure 18B for cutting plan, section 1 was located between axial grid lines 5-6, section 2 between grid lines 6-7 and section 3 between grid lines 7-9. All three sections were thoroughly cleaned ultrasonically in toluene and acetone prior to examination.

Section 1:

An enlarged macro view of this fracture section is shown in figure 20. It exhibited three distinct regions (A-C) as marked on the photograph. Each region was examined under a scanning electronic microscope (SEM).

Figure 21 - This low magnification fractograph shows region A near the last thread.

Figure 22 - It is from a location close to the last thread in region A, showing metal fold, formed during extrusion process, on the internal surface (near neck). It exhibits a featureless area.

Figure 23 - It is from a location deeper in region A. It shows a featureless fracture. Some evidence of localized dimpled rupture and grain boundary decohesion was also observed.

Figure 24 - It is from a location in region A (near region B). It also shows featureless regions as in figure 23, but dimpled regions and grain boundary separation are easily identifiable.

Figure 25 - It is from a location in region B. It shows featureless smooth facets as in figures 23 and 24. Well defined evidence of grain boundary decohesion was also observed.

Figure 26 - It is from a location in region C. It shows similar fractures as in figure 24.

Figure 27 - It is from a location in region C, farther away from location in figure 26. It exhibits clearly defined intergranular failure.

Sections 2 and 3:

Entire fracture areas in these sections exhibited intergranular failure in general. Dimpled rupture was also observed in certain areas. A typical fractograph is presented in Figure 28.

From examination of the fracture surfaces, it appears that the cracks initiated along extrusion folds on the internal surface in the thick section region near the last thread. Three regions of fracture (A, B, and C), discussed earlier in reference to fracture section 1, were formed during three separate one-time events characterized by two arrest marks boardering region B. Region C (third event) continued into fracture sections 2 and 3. None of the regions on the fracture surfaces exhibited any role of fatigue damage; each fracture region exhibited failure due to a single tension-type overload. The fracture surfaces revealed a mixed mode of failure of intergranular decohesion, some dimpled rupture and featureless regions probably formed due to transgranular failure as discussed in the metallographic analysis section.

METALLOGRAPHIC EXAMINATION

One transverse and one longitudinal section, each near the fracture surface and remote from it, were cut for micro-metallographic examination. The section locations are shown in figure 29. A section consisting of the neck and barrel regions was also prepared for macroanalysis; location of this section is shown in figure 30.

MACRO-ANALYSIS:

The macro section outlined in figure 30 was lapped up to 600 grit paper and etched with Keller's reagent. The overall macrograph of the section is shown in figure 31. It exhibits fine grain structure in the barrel region; grain size slowly becomes large towards the neck region. Areas marked 1, 2, and 3 were photographed at a larger magnification which clearly indicate significant difference in grain size between the neck and barrel regions; see figures 32-34. The material in the neck region appears to have undergone recrystallization and appreciable grain growth; no apparent grain growth was observed in the barrel region.

MICRO-ANALYSIS:

The sections outlined in figure 29 were prepared for micro-analysis. Typical photomicrographs exhibiting microstructures of the inside and outside surfaces of the longitudinal sections L1 and L2 are presented in figures 35 and 36, respectively.

Figure 35: The micrographs representing the inside and outside surfaces show flow lines formed during the extrusion process. The inside surface appears to have much finer grains as compared to the outside surface.

Figure 36: Extrusion flow lines seen in the barrel region (figure 35) were not present in the neck region. The micrographs representing the neck region indicate that material in that area underwent recrystallization and extensive grain growth throughout the section. Both the inside and outside surfaces exhibited a similar microstructure having very coarse grains relative to the barrel region.

The presence of some coarse particles was observed both along grain boundaries and inside grains in figures 35 and 36. These particles were later detected to have substantial presence of Pb and Bi; see metallographic analysis section.

Examination of Section L2:

Figure 37: This is a micrograph showing areas near the fracture face. Examination along the fracture face revealed an intergranular and transgranular mixed mode failure. Intergranular failure is attributed to weakened grain boundaries (white regions in the micrographs) due to the presence of Pb and Bi. Weakness of the grain boundaries is shown by a Knoop microhardness indentation in figure 38; half of the indentation falling in white region is larger than the other half in the dark region indicating that the white area is softer than the dark area. A likely cause of transgranular failure is due to the presence of crack initiation sites offered by some Pb - Bi particles trapped inside grains, which could have occurred during the recrystallization process.

Figure 39: It shows internal cracks running almost parallel to the main crack front. It is attributed to inherent weaknesses in the material mentioned in figure 37 description which caused cracks to initiate under tensile load (Hoop stress) while the cylinder was under pressure.

Figure 40: Coarse particles observed along grain boundaries and inside grains were analyzed using energy dispersive spectrometer (EDS). The SEM micrograph showing the analyzed spot

and the EDS spectrum are presented in figure 40; it indicates a strong presence of Pb along with Fe and Mn (figure 40B). Another spot analysis revealed the presence of Bi (figure 40C).

Examination of Section L1:

Coarse particles observed in figure 35 were analyzed using EDS. The SEM micrograph showing the analyzed spot and the EDS spectrum are presented in figure 41. It indicates a strong presence of Pb in the material.

Examination of metallographic sections confirmed the presence of an appreciable amount of Pb and Bi detected during chemical analysis. It also confirmed results of fracture examination which indicated a mixed mode failure occurring under a tensile load (Hoop stress).

MICROHARDNESS TESTING

Microhardness testing was performed across sections L1 and L2. Measured range of hardness for L1 was 116-118 HV and that for L2 was 112-117 HV. These values represented a T6 temper for Al 6351 alloy.

1

2

3

4

Figures 1-4: As-received views of the subject cylinder's general conditions, identification markings and an overall view of the fracture surfaces.

5

6

7

8

Figure 5-8: As-received views of the subject cylinder showing manufacturer's name Luxfer USA (Figure 5) and other identifying markings.

9A

9B

10

Figures 9-10: As-received views of the cylinder showing identification markings on its bottom (figure 9), caution sticker, and date of internal inspection (figure 10).

11. X 0.5 approx.

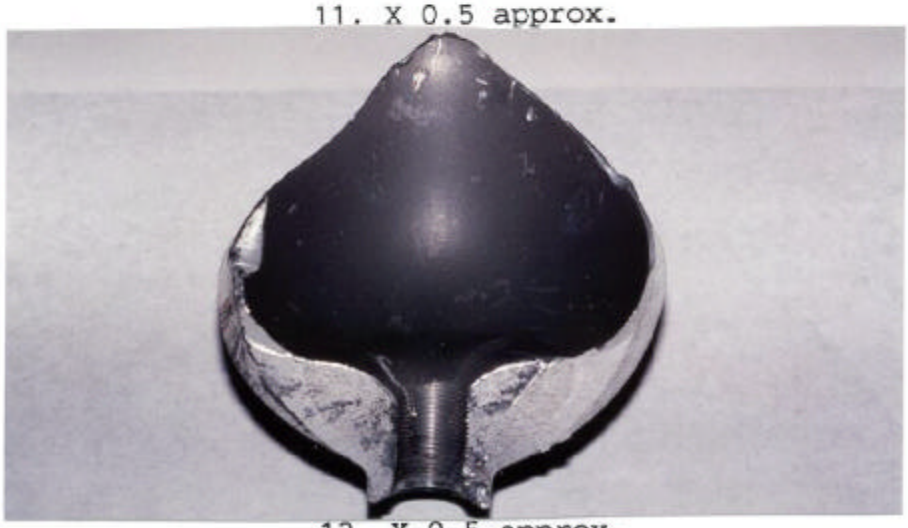

12, X 0.5 approx.

13, X 2 approx.

Figure 11-13: As-received views of two smaller pieces of fracture.

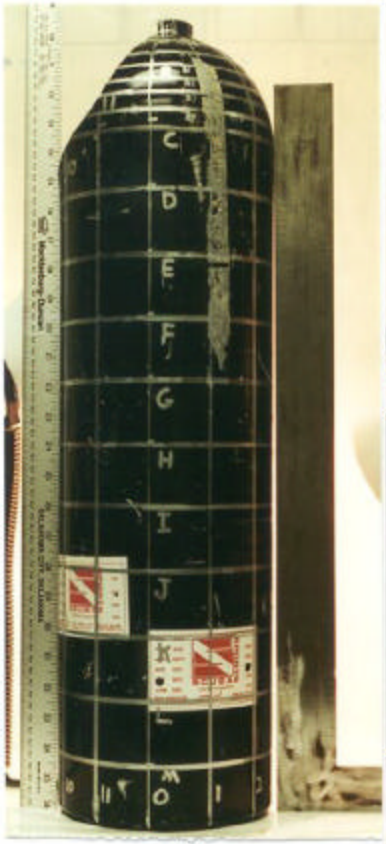

14

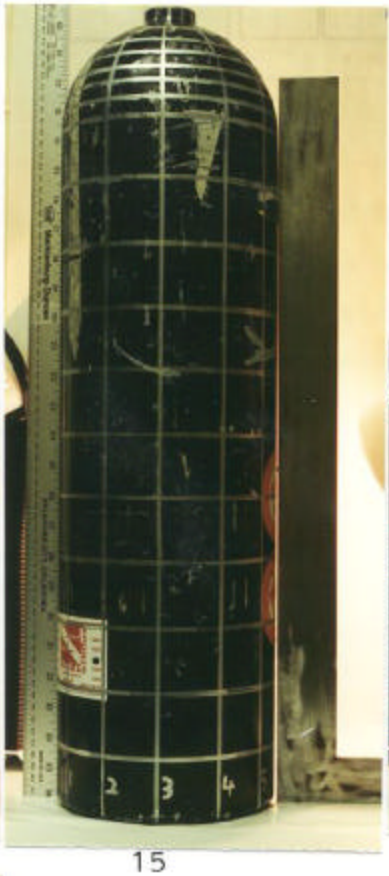

15

16

17

Figure 14-17: Photographs exhibiting the grid layout. They also show overall straightness of the cylinders. There appears to be slight bulging near the base of the dome part of the cylinder.

Figure 18A: Locations of chemical samples from near OC grid point (small arrow), and from near OA2 grid point (large arrow).

Figure 18B: View of the fractured dome part cut from the cylinder. It shows locations of fracture surface sections 1, 2 and 3, which were removed for examination.

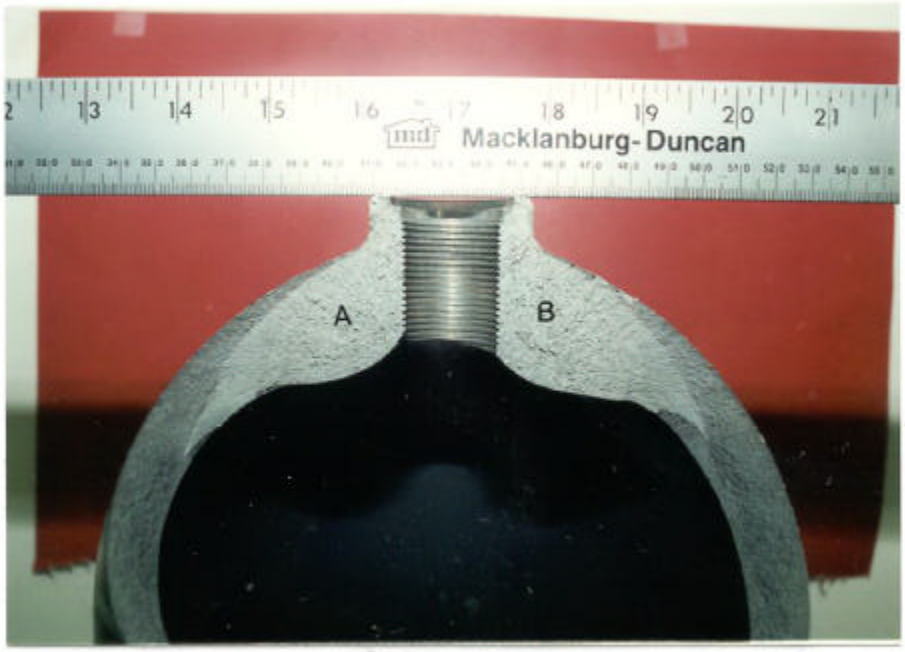

Figure 19: A macro view of the fracture surface. Side A was used for fractography and side B for metallography.

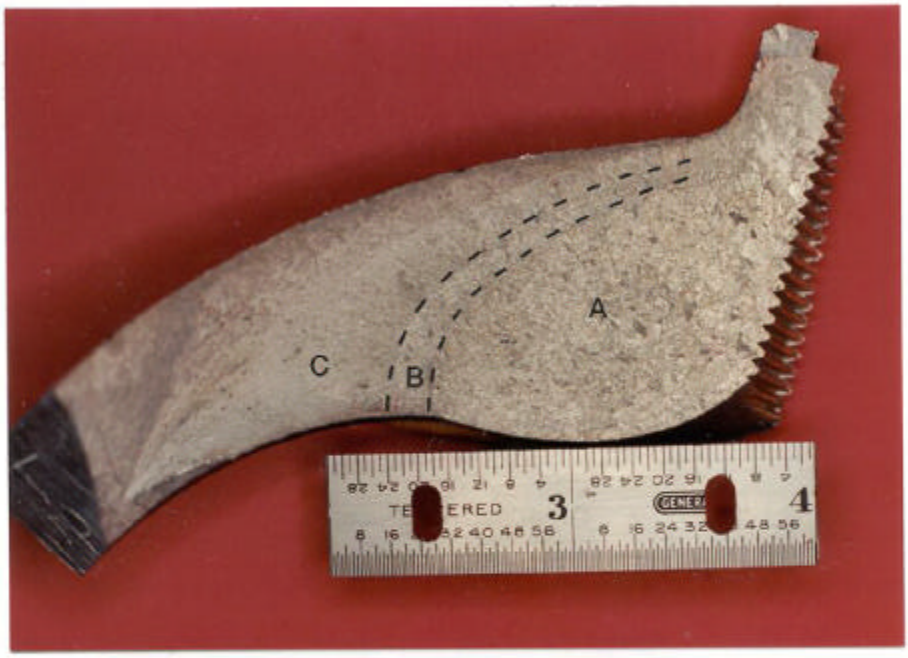

Figure 20: An enlarged view of section 1 (figure 18B) shows three distinct regions on the fracture surface marked A, B and C.

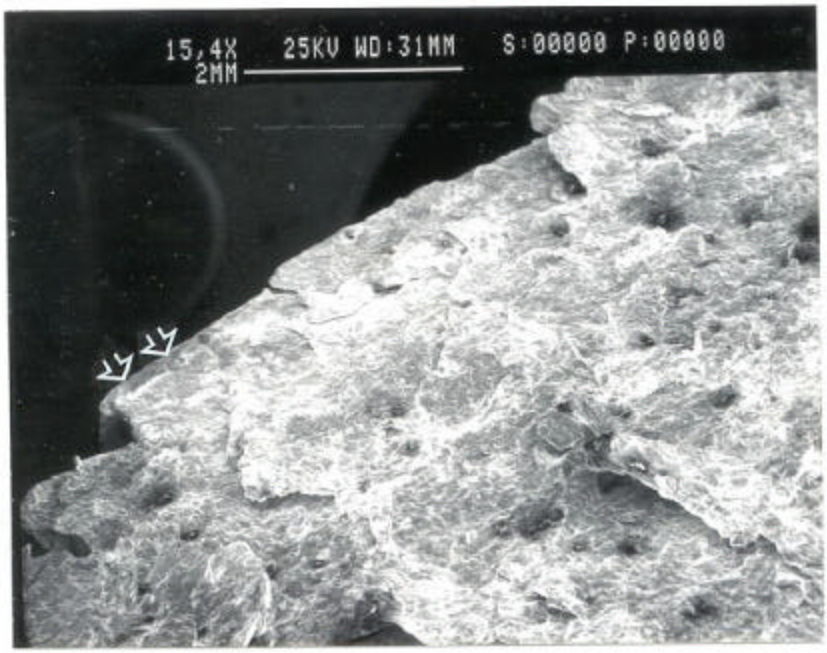

Figure 21: A low magnification SEM fractograph of region A shows areas near the last thread, X15.

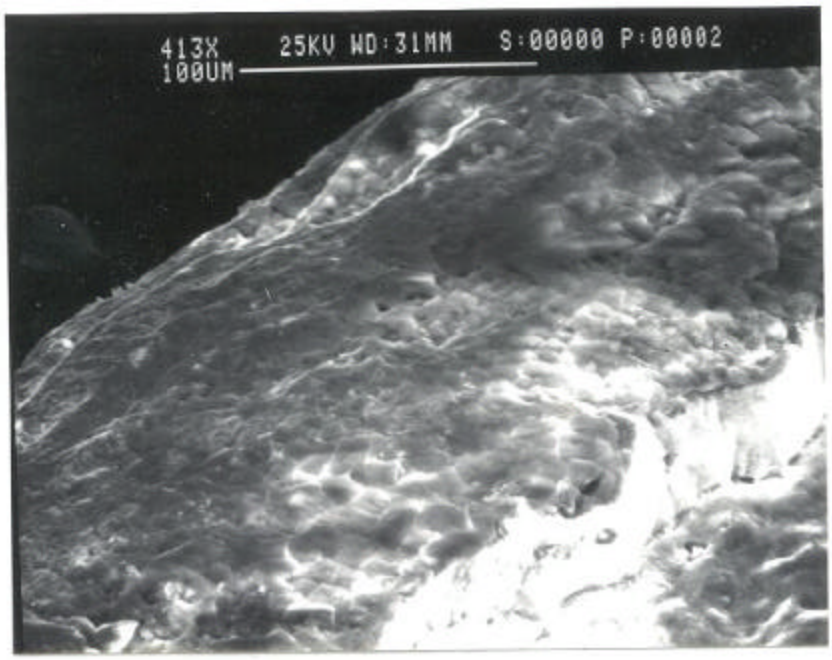

Figure 22: Enlarged view of the edge indicated by arrows in Figure 21, exhibits a featureless metal fold formed during extrusion process, X413.

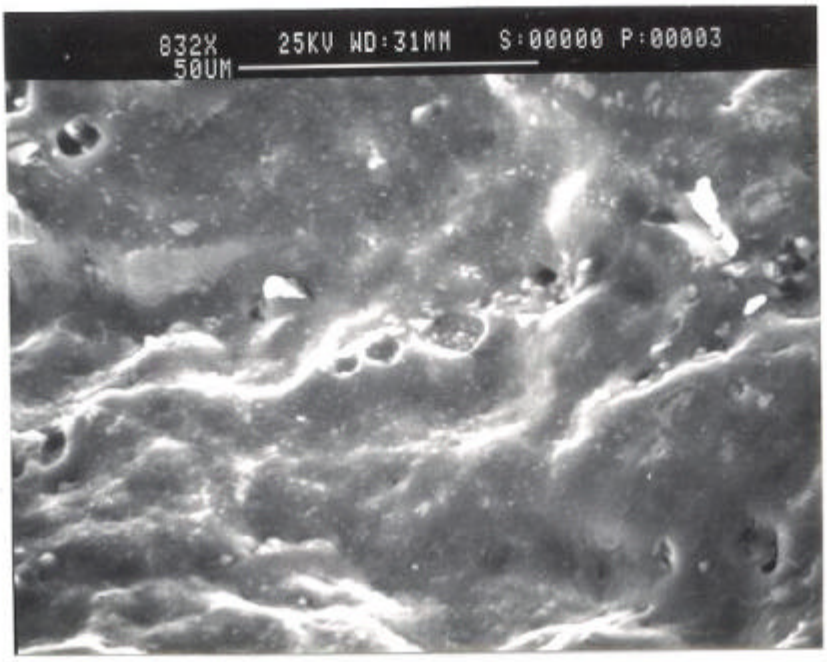

Figure 23: Fractograph of an area deeper in region A shows featureless fracture. Some evidence of dimpled rupture and intergranular failure was also observed, X832.

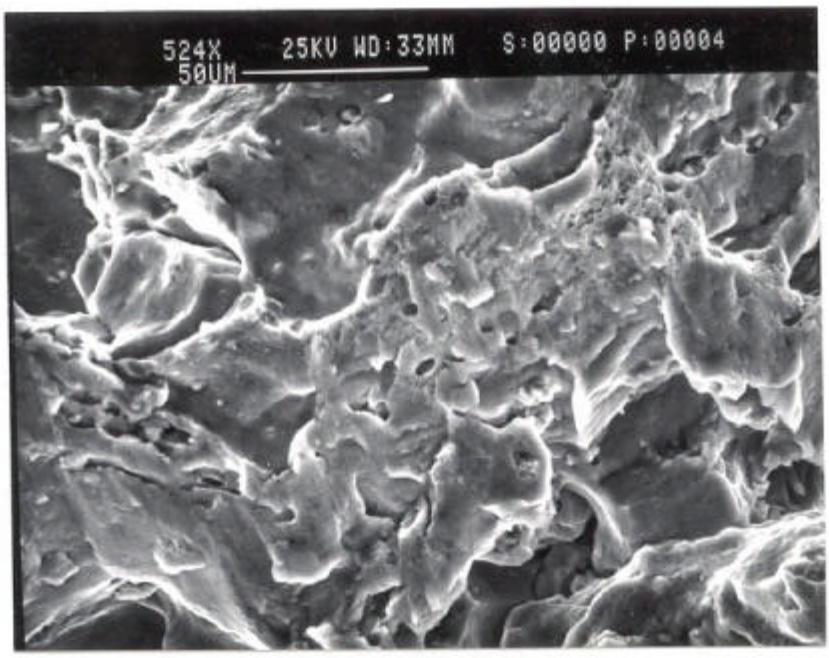

Figure 24: Fractograph from an area in region A (near region B) is featureless as in figure 23. However, evidence of dimpled rupture and grain boundary decohesion is more decernible, X524.

Figure 25: Fracture in region B exhibited featureless regions. It also clearly indicated evidence of grain boundary failure, X663.

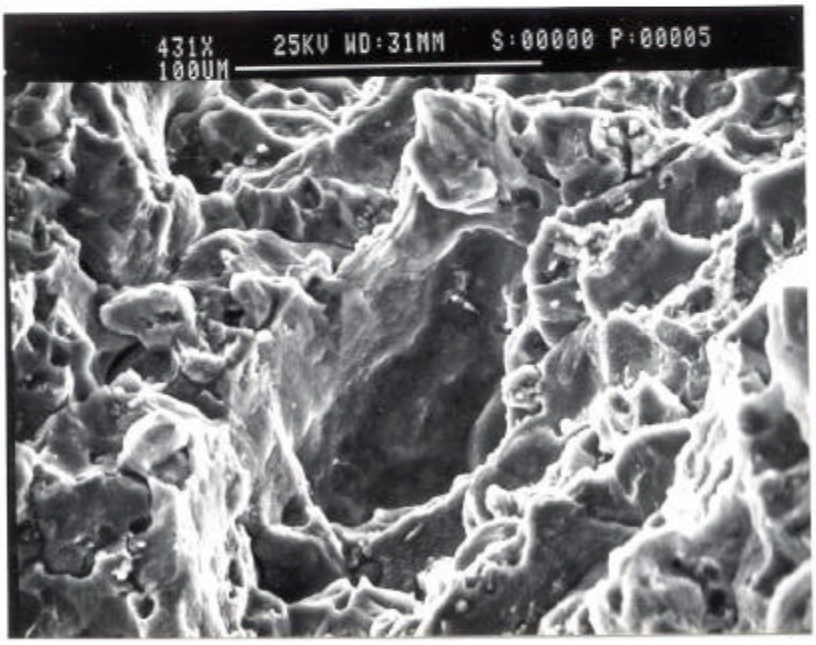

Figure 26: Fractograph from an area in region C. It shows similar features as in figure 24.

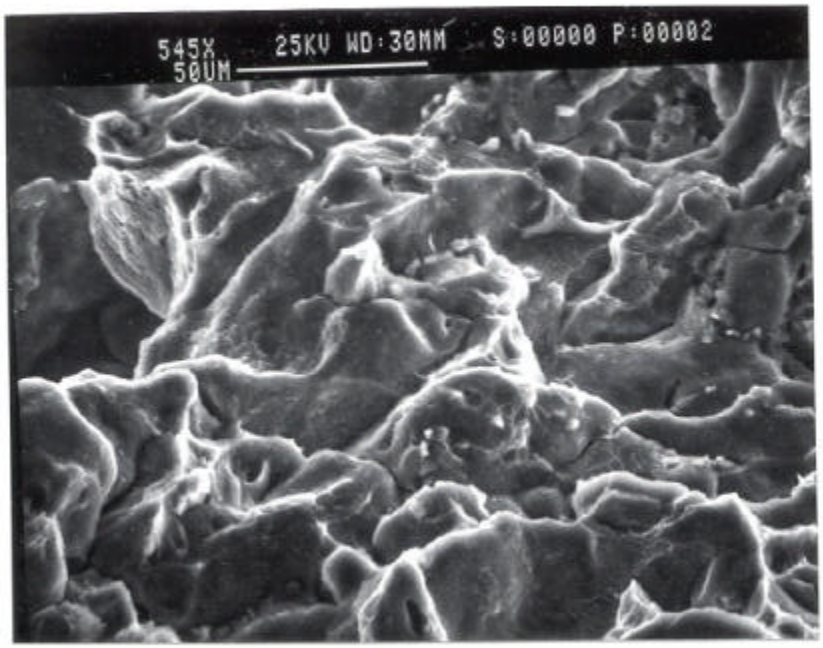

Figure 27: Fractograph from an area deeper in region C. It exhibits clearly defined intergranular failure, X545.

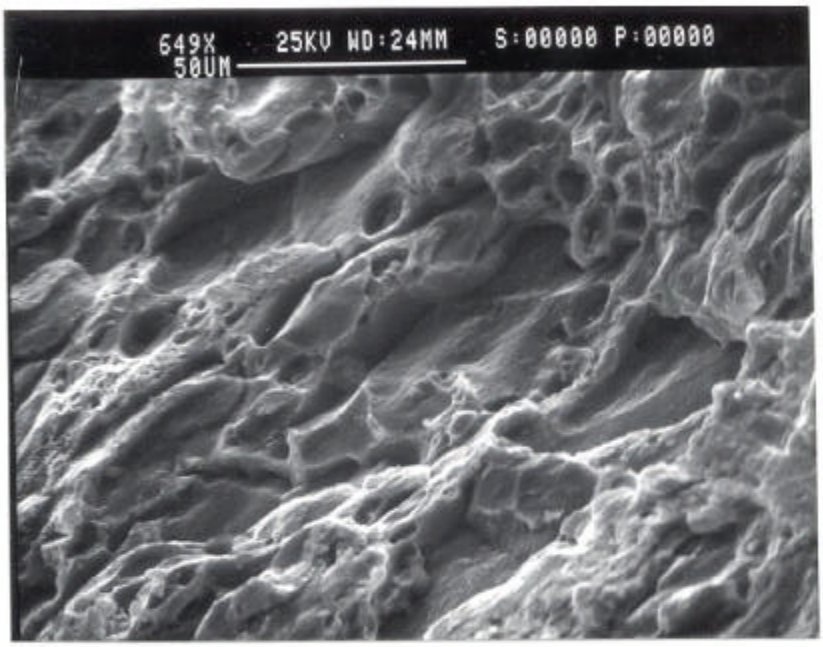

Figure 28: A typical fractograph of the fracture surface in sections B and C showing largely intergranular failure. Some evidence of dimpled failure can also be observed, X649.

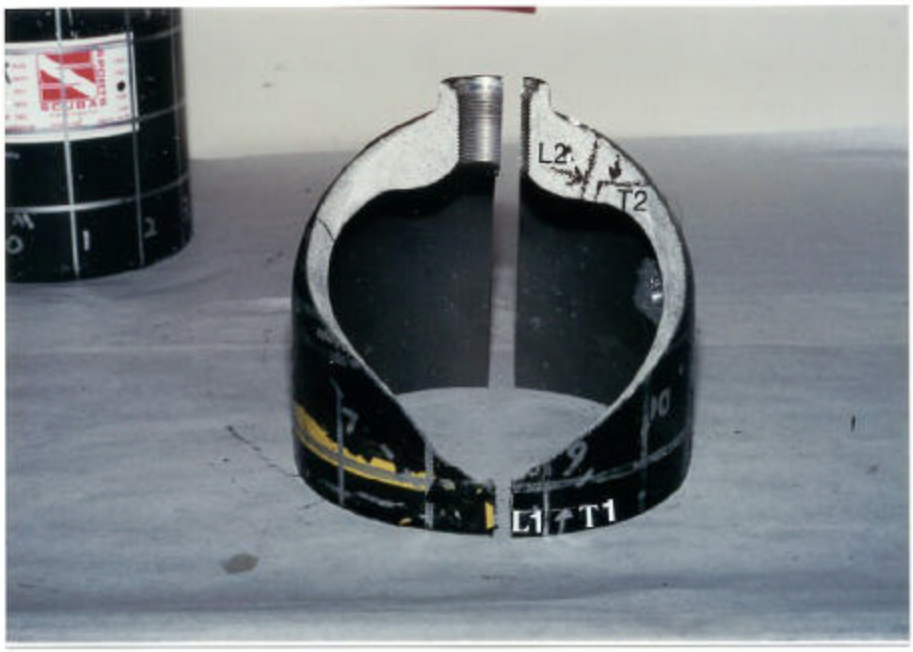

Figure 29: Locations of longitudinal (L1 and L2) and transverse (T1 and T2) sections cut for metallographic examination, shown by arrows.

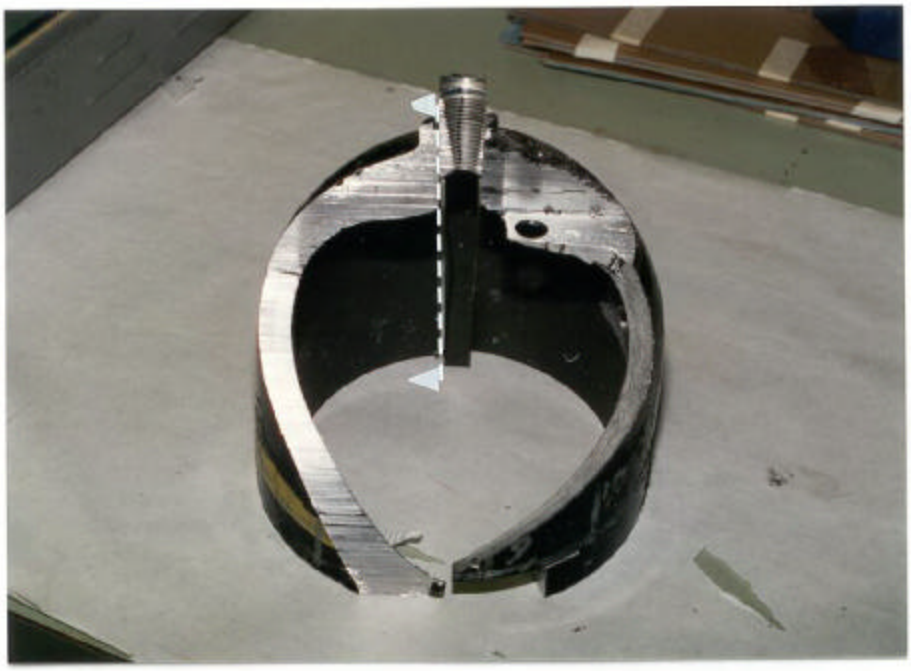

Figure 30: Photograph indicating the section used for macro analysis.

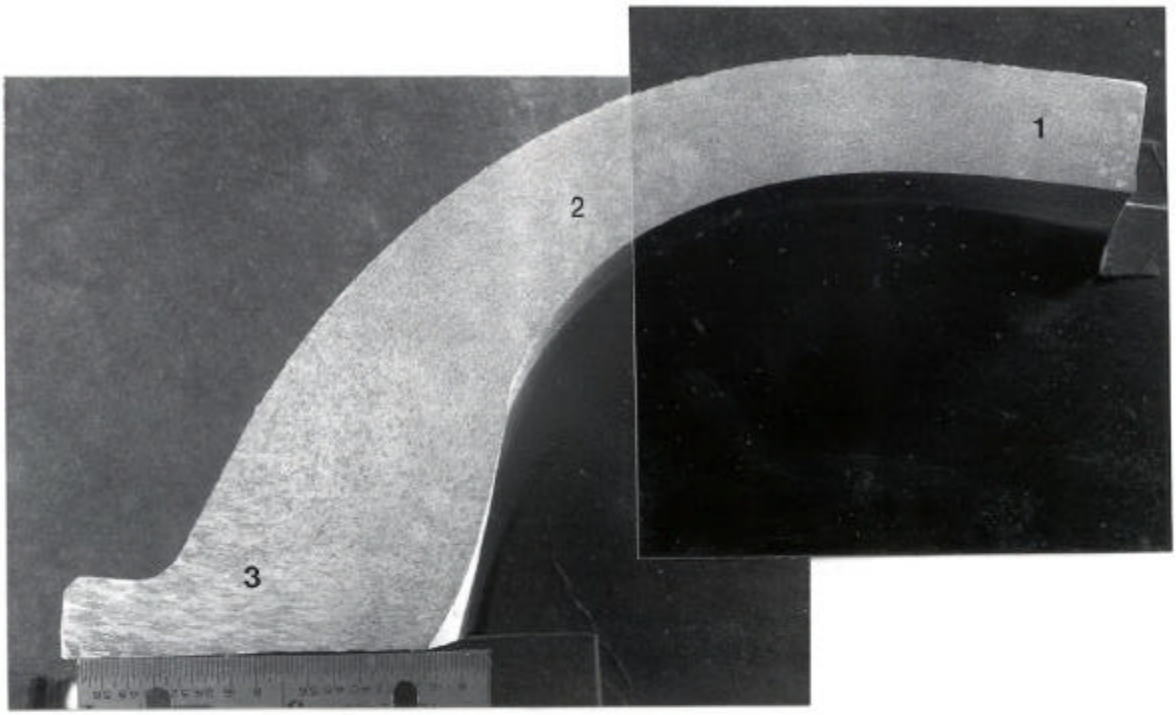

Figure 31: Macrophotograph of the section indicated in figure 30. It exhibits fine grain structure in the barrel section and coarse grains near the neck region, X1.14, Keller's Etch.

Section 32: Enlarged view of the area marked 1 in figure 31 shows a very fine grain size, X10.

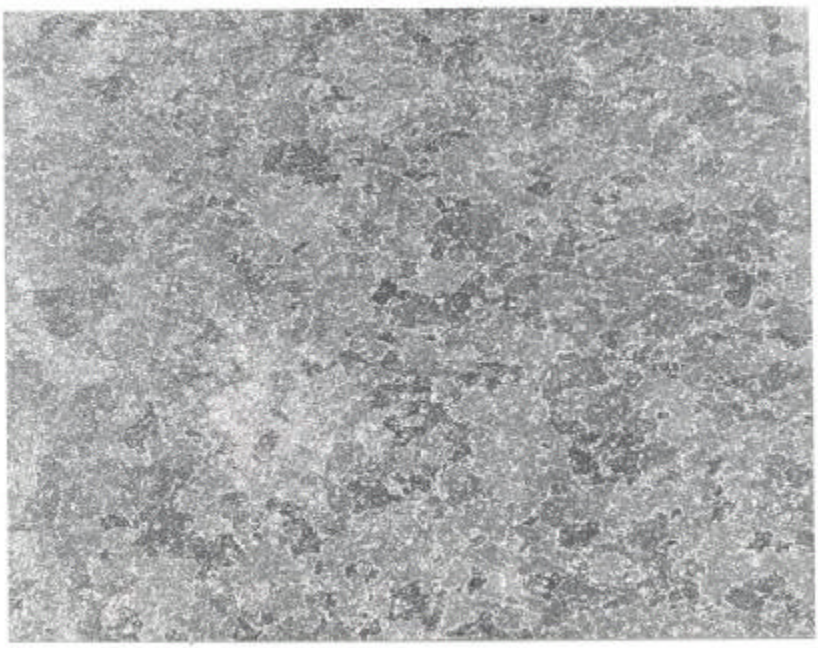

Figure 33: Enlarged view of the area marked 2 in figure 31 shows coarse grains as compared to those shown in figure 32, X10.

Figure 34: Enlarged view of the area marked 3 in figure 31 shows coarse grains as compared to those shown in figure 33, X10.

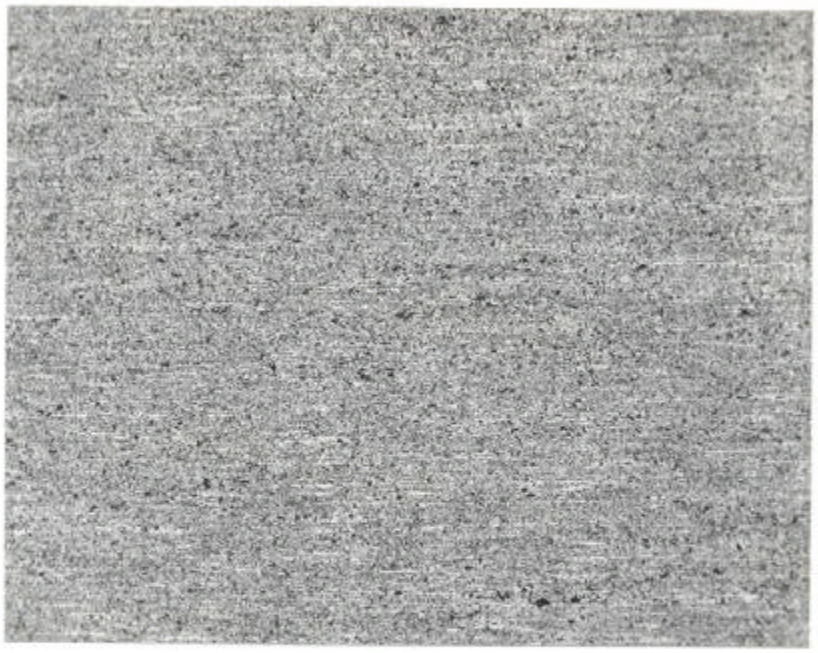

A

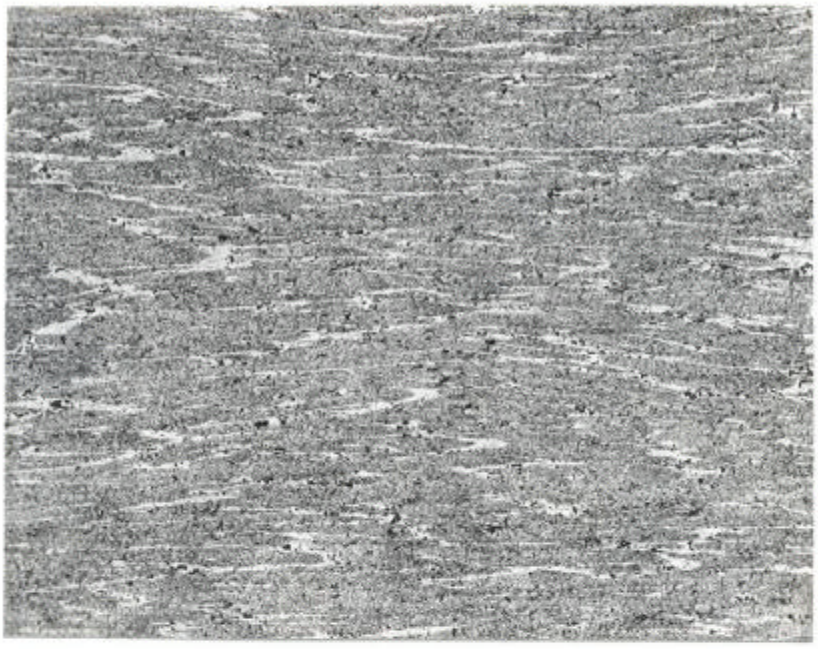

B

Figure 35: Photomicrographs showing microstructures near the inside surface (A) and near the outside surface (B). Extrusion flow lines are apparent. Grain size near the inside surface appears to be much finer as compared to that near the outside surface, X100.

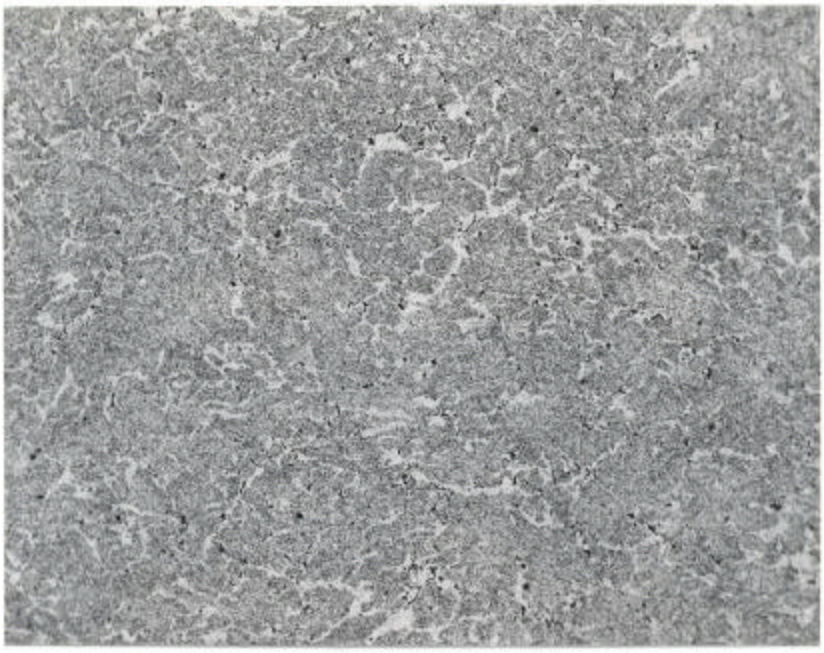

A

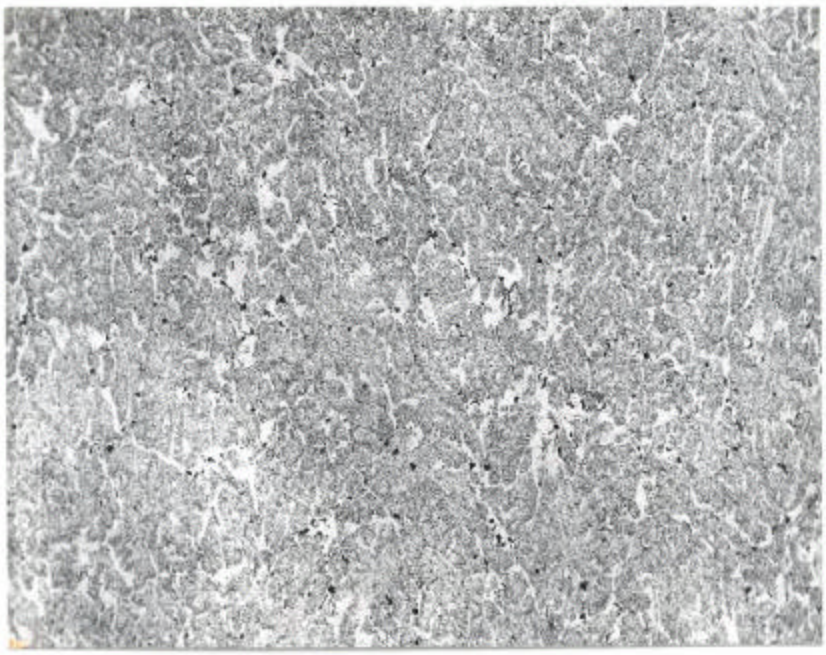

B

Figure 36: Photomicrographs showing microstructures near the inside surface (A) and near the outside surface (B). No extrusion flow lines are present. They exhibit extensive grain growth in the area. Some precipitate particles can be seen along grain boundaries and inside grains, X100.

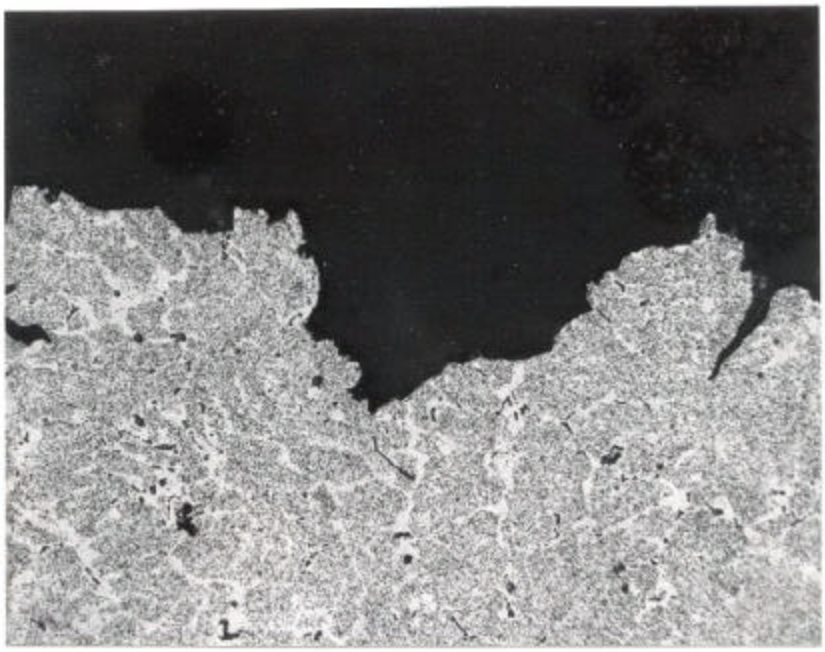

Figure 37: Photomicrographs showing the microstructure along the main crack front. It indicates a mixed mode fracture consisting of intergranular and transgranular failure, X200.

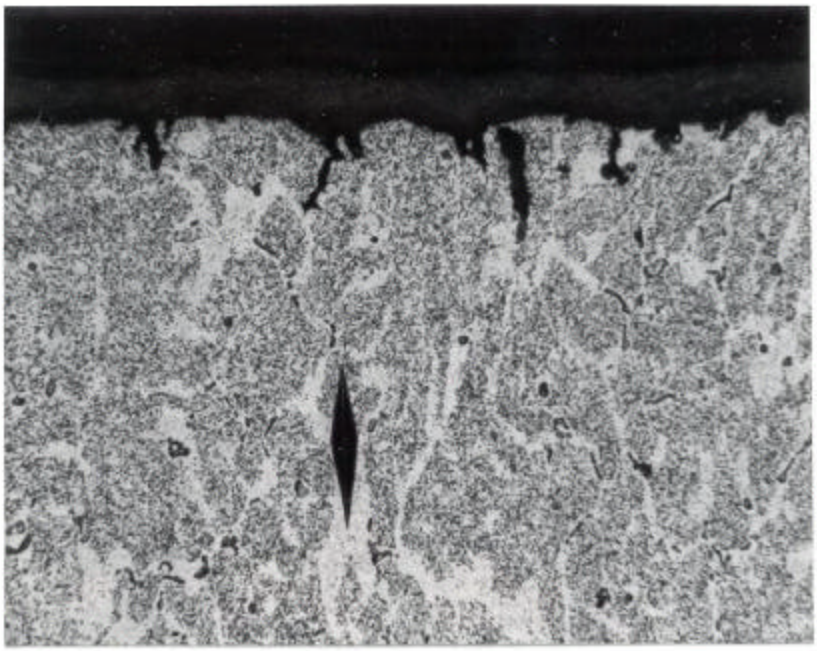

Figure 38: Photomicrograph exhibits a Knoop microhardness indentation showing its half diagonal located in the white region larger than the other half in the dark region, X300.

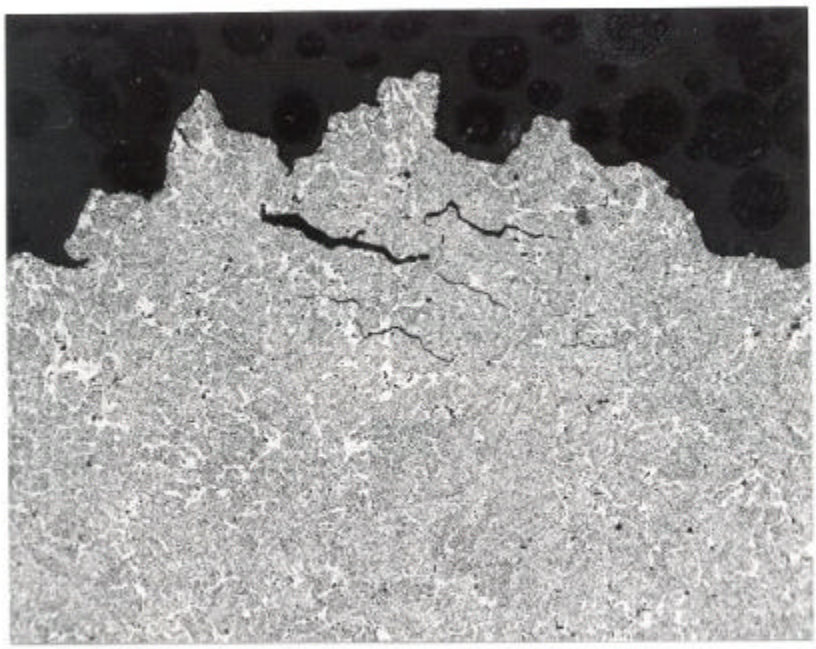

Figure 39: Photomicrograph shows internal cracks running parallel to the main crack front, X100.

Figure 40A: SEM micrograph exhibits the spot on a precipitate particle which was analyzed using EDS, X3390.

EG&G Ortec System 5000
Spectrum Plotting Program
Printplot V02.05

Sample ID: J9509.002;Mount #8150-Particle

Energy Range: 0 - 20 keV 10 eV/ch Hi Res

Preset: Off

Real Time: 388.37 Sec. Live Time: 50.08 Sec.

88% Deadtime 44373 Counts/Second

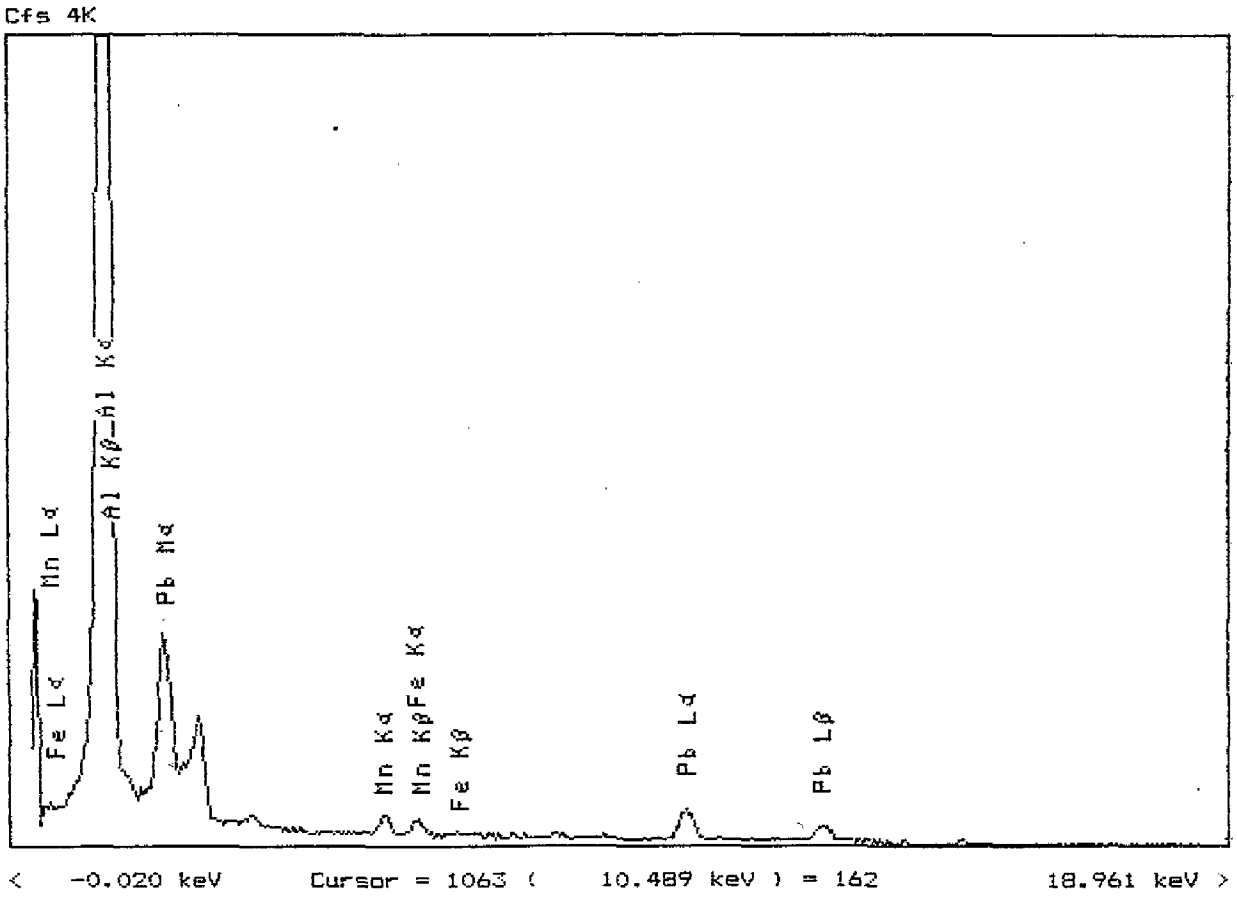

Figure 40B: EDS spectrum of the spot shown in figure 40A indicates the presence of Pb, Mn, and Fe.

EG&G Ortec System 5000
Spectrum Plotting Program
Printplot V02.05

Sample ID: J9509.002;Mount #8150-Particle

Energy Range: 0 - 20 keV 10 eV/ch Hi Res

Preset: Off

Real Time: 345.28 Sec. Live Time: 50.10 Sec.

85% Deadtime 44623 Counts/Second

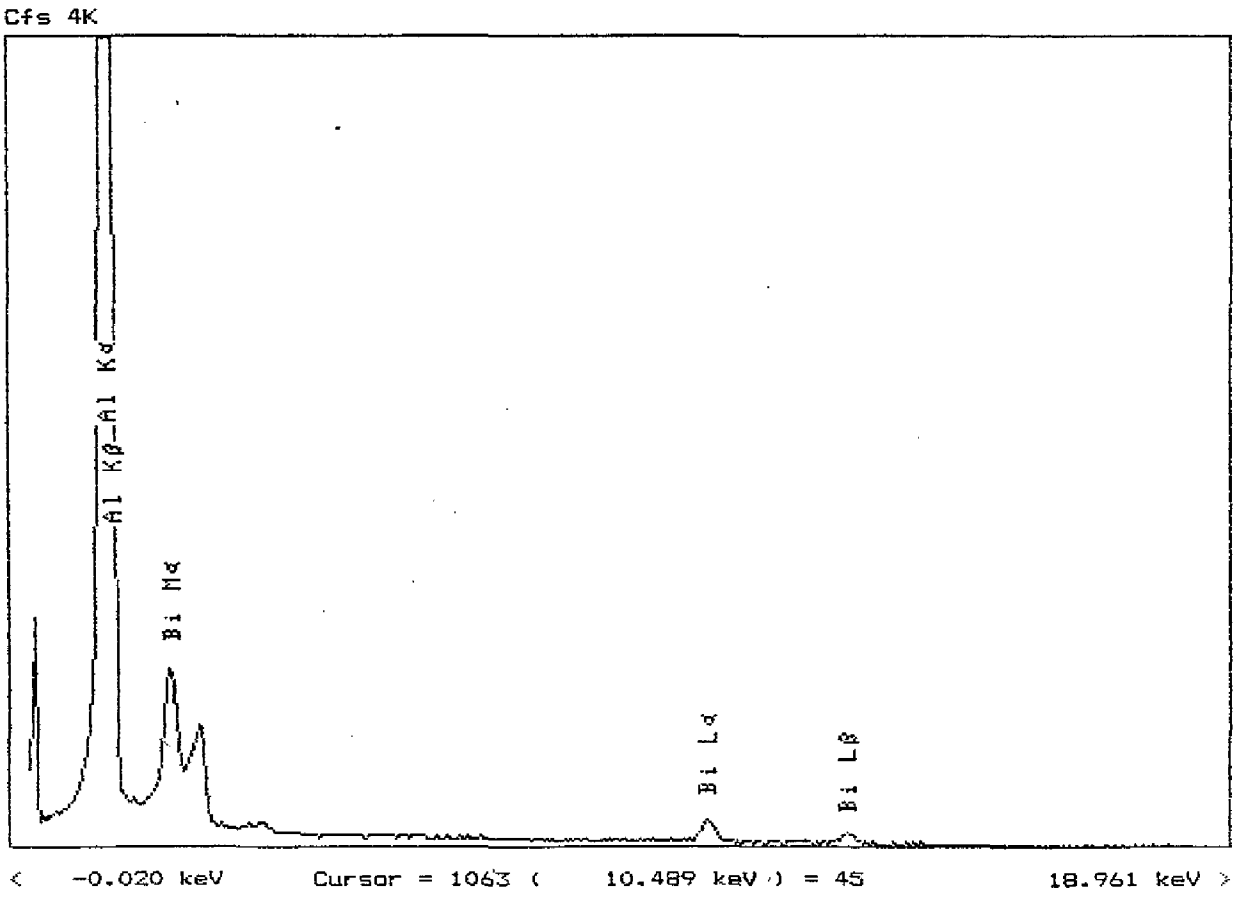

Figure 40C: EDS analysis of another spot on the same mount as in figure 40A detected appreciable presence of Bi.

Figure 41A: SEM micrograph showing the spot on a precipitate particle which was analyzed using EDS, X5850.

EG&G Ortec System 5000
Spectrum Plotting Program
Printplot V02.05

Sample ID: J9509.002;Mount #8152-Particle

Energy Range: 0 - 20 keV 10 eV/ch Hi Res

Preset: Off

Real Time: 286.00 Sec. Live Time: 50.12 Sec.

83% Deadtime 43068 Counts/Second

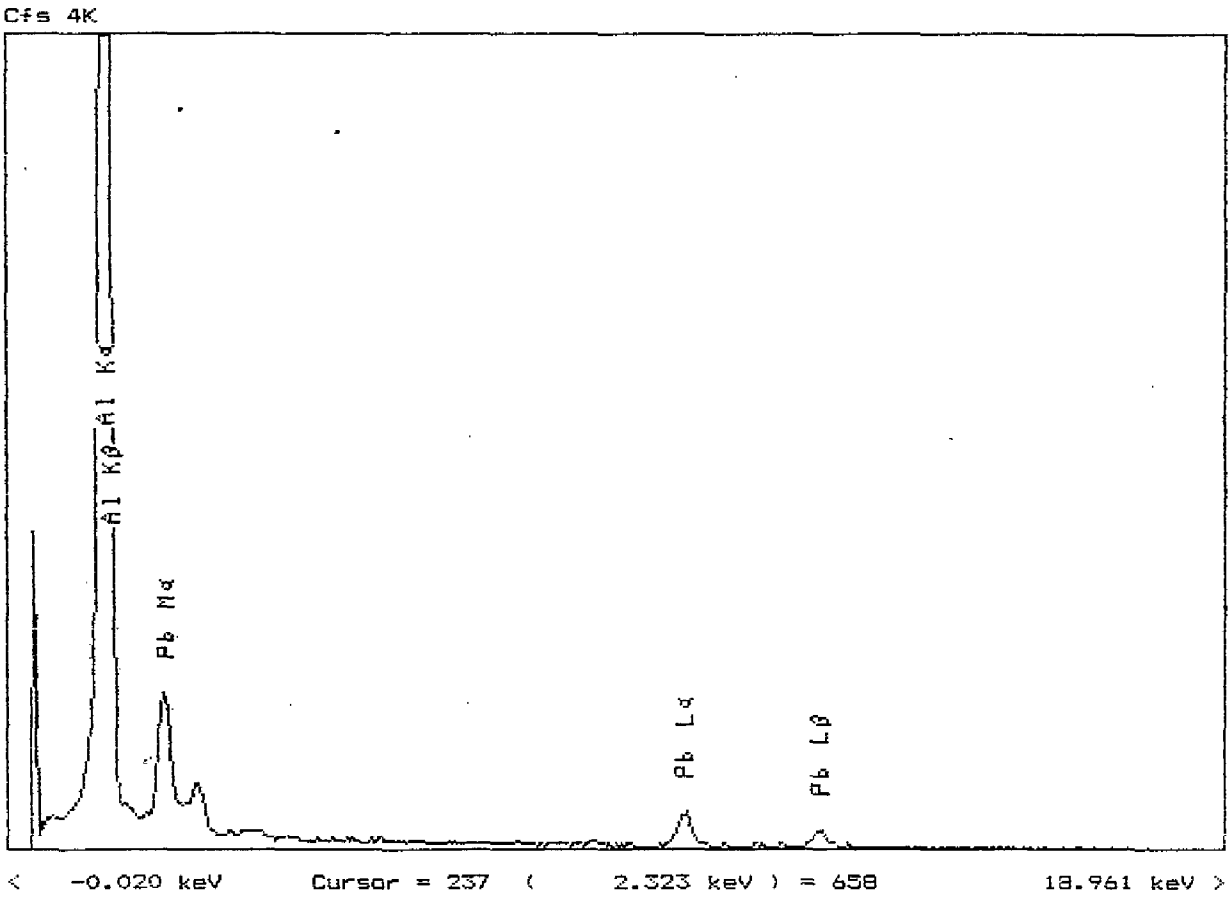

Figure 41B: EDS spectrum of the spot shown in figure 41A shows the presence of Pb.

Appendix I

CHAIN OF CUSTODY FORM

ARTECH CORP

14554 Lee Rd
Chantilly, Va 22021

Phone (703) 378-7263
Metro (703) 968-8378
Fax (703) 378-7274

ARTECH Job Number 9509.002

Client: U. S. DOT/RSPA — Client Job Number
Address: 400 7th Street, S.W.
Washington, D.C. 20590-0001
Contact: Gopalo Vinjumari
Phone #: 202-364-4545 FAX #:

Sampled By: Sampling Date:

Sample # and Location	Analysis Required	Sampling Date & Time	Volume of Sample & Matrix	Preservatives and Remarks
P20860	DTRS56	9/28/94	25 inch long	CTC/DOT-3AL-3000
	-94-P-	1400	6-7 in OD	-11A82
	70365			

Released by:	Date & Time	Received by:	Date & Time
GOPALA K VINJAMURI DOT/RSPA DHM-22	9/28/94 2:30PM	PAUL J LARE	9/28/94-1400
Released by:	Date & Time	Received by:	Date & Time
Received in lab by:	Date & Time	Method of shipment:	

Appendix II

Lead Analysis Procedures

ARTECH uses a Buck Scientific Model 200 A Atomic Absorption Spectrometer (AAS) with flame aspiration for the analysis of lead in metals. The metal is digested using standard procedures (nitric acid being the most common digestion to avoid the low solubility of lead chloride). Standard solutions of lead in a matrix matched solvent (use of acid at the same concentration as the metal digestion to eliminate effects from variations in the viscosity of the solutions) are made from NIST traceable standard solution concentrates. The typical standards are 5, 10 and 20 parts per million in solution.

The procedure used for the analysis is as specified in EPA 7420. A lead hollow cathode lamp is used as the light source. An acetylene-air flame is used. The 283.3 nm line is used. Calibration by "Methods of Addition" is used for any sample which has a possible interference due to materials in the sample.

Chemical interferences with lead can include the presence of chromate, which causes a precipitation of lead chromate, the presence of sulfide which precipitates lead sulfide, and the presence of high levels of chloride which precipitates lead chloride. Any precipitation of a metal in a digested sample removes that metal from the solution and thus from the analysis.

Bismuth Analysis

ARTECH uses a Buck Scientific Model 200 A Atomic Absorption Spectrometer (AAS) with flame aspiration for the analysis of bismuth in metals. The metal is digested using standard procedures (nitric acid being the most common digestion to avoid the low solubilities of some metal chlorides). Standard solutions of bismuth in a matrix matched solvent (use of acid at the same concentration as the metal digestion to eliminate effects from variations in the viscosity of the solutions) are made from NIST traceable standard solution concentrates. The typical standards are 5, 10 and 20 parts per million in solution.

The procedure used for the analysis is as specified in the Perkin-Elmer "Cookbook", method Bi 1. A bismuth hollow cathode lamp is used as the light source. An acetylene-air flame is used. The 223.1 nm line is used. Calibration by "Methods of Addition" is used for any sample which has a possible interference due to materials in the sample.

Tin Analysis Procedures

ARTECH uses a Buck Scientific Model 200 A Atomic Absorption Spectrometer (AAS) with flame aspiration for the analysis of tin in metals. The metal is digested in an appropriate acid, typically nitric acid. Standards of 20, 50, and 100 parts per million are prepared from NIST traceable concentrates. The flame is set with a fuel rich mixture to give maximum absorption at a known tin concentration in the standard. If the amount of tin in the sample is below 20 parts per million in solution, the sample is spiked with a known amount of tin and the reading corrected for this spike.

The procedures used for tin are from the Perkin-Elmer "Cookbook, Method Sn 1. A tin hollow cathode lamp at 12.0 mA, a slit of 2A, and a wavelength of 2863A is used for the analysis.

Specific Procedures, Aluminum Cylinder Analysis

A one gram sample of metal turnings, removed from the core of the sample and solvent washed to remove traces of cutting oil and fingerprints, was dissolved using 25 mL of water and 10 mL of 3N Nitric acid. The resulting solution was taken to 100 mL total volume with deionized water. This solution was analyzed using the standard AAS procedures for lead, bismuth, and tin. The samples were found to be comparable in absorption to the 5 ppm lead standard solution (for lead), comparable to the 5 ppm bismuth standard (for bismuth) and were found to be slightly less than the 20 ppm tin standard (for tin). The expected precision of these measurements are 5% of value.